

See discussions, stats, and author profiles for this publication at: <https://www.researchgate.net/publication/263944521>

# Spectroscopic characterization of Ca<sub>3</sub>Y<sub>2</sub>Si<sub>3</sub>O<sub>12</sub>:Eu<sup>2+</sup>,Eu<sup>3+</sup> powders in VUV–UV–vis region

ARTICLE *in* THE JOURNAL OF PHYSICAL CHEMISTRY C · NOVEMBER 2012

Impact Factor: 4.77 · DOI: 10.1021/jp306764f

---

CITATIONS

16

---

READS

44

## 2 AUTHORS:



Anna Dobrowolska  
Delft University of Technology

20 PUBLICATIONS 61 CITATIONS

[SEE PROFILE](#)



Eugeniusz Zych  
University of Wroclaw

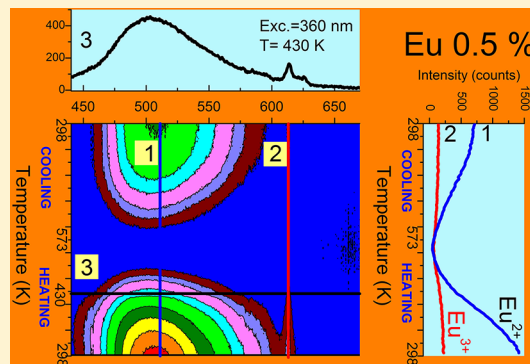
172 PUBLICATIONS 1,738 CITATIONS

[SEE PROFILE](#)

# Spectroscopic Characterization of $\text{Ca}_3\text{Y}_2\text{Si}_3\text{O}_{12}:\text{Eu}^{2+},\text{Eu}^{3+}$ Powders in VUV-UV-vis Region

Anna Dobrowolska<sup>†</sup> and Eugeniusz Zych<sup>\*,†,‡</sup><sup>†</sup>Faculty of Chemistry, University of Wroclaw, 14 F. Joliot-Curie Street 50-383 Wroclaw, Poland<sup>‡</sup>Wroclaw Research Centre EIT+, 147 Stablowicka Street 54-066 Wroclaw, Poland

**ABSTRACT:**  $\text{Ca}_3\text{Y}_2\text{Si}_3\text{O}_{12}$  powders activated with Eu (0.1–25%) were prepared by means of ceramic method. Their spectroscopic properties in VUV-UV-vis region were investigated. Luminescence measurements indicated that  $\text{Ca}_3\text{Y}_2\text{Si}_3\text{O}_{12}$  prepared in a strongly reducing atmosphere of 20% $\text{N}_2$ –80% $\text{H}_2$  mixture contained both  $\text{Eu}^{2+}$  and  $\text{Eu}^{3+}$  ions, and both were able to generate their characteristic emissions. A superposition of the broad band luminescence of  $\text{Eu}^{2+}$  and narrower 4f → 4f luminescent features of  $\text{Eu}^{3+}$  upon excitation with 395 nm light-emitting diode covered almost the whole visible part of spectrum. The ratio between  $\text{Eu}^{2+}$  and  $\text{Eu}^{3+}$  emissions was reproducible, and, with increasing content of Eu, the relative intensity of the red component from  $\text{Eu}^{3+}$  became systematically stronger. The  $\text{Eu}^{2+}$  luminescence in  $\text{Ca}_3\text{Y}_2\text{Si}_3\text{O}_{12}$  was characterized by an extraordinary large Stokes shift of  $\sim 8960 \text{ cm}^{-1}$  and most probably had an anomalous character with a defect, presumably O-vacancy located in the vicinity of  $\text{Eu}^{2+}$ , being involved in the emission generation. Excitation into the VUV-UV region with synchrotron radiation revealed that at 10 K, despite  $\text{Eu}^{3+}$  and  $\text{Eu}^{2+}$  ions, two kinds of intrinsic emissions, peaking around 340 and 420–440 nm, contributed to the luminescence of  $\text{Ca}_3\text{Y}_2\text{Si}_3\text{O}_{12}:\text{Eu}$ . Luminescence measurements in the range of 293–573 K and decay kinetics of  $\text{Eu}^{3+}$  and  $\text{Eu}^{2+}$  emissions revealed that the continuously decreasing fraction of  $\text{Eu}^{2+}$  ions contributed to the emission with increasing temperature, yet the thermal quenching of emission monitored by changes in its decay time could merely be seen above 500 K. The unusual temperature behavior of  $\text{Eu}^{2+}$  luminescence in  $\text{Ca}_3\text{Y}_2\text{Si}_3\text{O}_{12}:\text{Eu}^{2+},\text{Eu}^{3+}$  was assigned to the instability of exciton-like state diffused over [ $\text{Eu}^{2+}\text{-O}_{\text{vac}}$ ] defect cluster involved in the luminescence of  $\text{Eu}^{2+}$ . Although the performance of the phosphor was not optimized, 40–44% of the quantum efficiency of the overall luminescence upon near-UV excitation was measured, proving its high potential.



## INTRODUCTION

Extraordinary energy efficiency, reasonable cost, long lifetime, and environmental friendliness make white light-emitting diodes (WLEDs) the most promising light source in general lighting and displays for the future.<sup>1</sup> A vast number of papers gave detailed descriptions of different methods of creating white light.<sup>2–12</sup> Nowadays, the most promising method employs phosphor materials as a medium converting the radiation from the primary source (LED) into visible light (it is called phosphor-converted white LED, pc-WLED).<sup>13,14</sup> YAG:Ce commercially used for that purpose currently has important drawbacks,<sup>13,15</sup> which stimulate studies on new materials and concepts. We try to contribute to this research, exploring a possibility of making a single phosphor material of low cost and capable of producing white light with spectral characteristics similar to sunlight. We consider using a near UV-LED (340–400 nm) as the primary excitation source for the calcium yttrium silicate,  $\text{Ca}_3\text{Y}_2\text{Si}_3\text{O}_{12}$ , host-doped with both  $\text{Eu}^{2+}$  and  $\text{Eu}^{3+}$  ions. We assumed that under favorable conditions of the material fabrication, Eu would tend to enter the host as a broad band emitting  $\text{Eu}^{2+}$ , whose 5d → 4f luminescence might locate in the bluish-green part of spectrum,

and  $\text{Eu}^{3+}$ , which generates photons in the orange-red region due to the 4f → 4f transitions.

Ca and Y randomly occupy three different symmetry sites present in the  $\text{Ca}_3\text{Y}_2\text{Si}_3\text{O}_{12}$  host. Upon doping, this complicates the luminescence properties of the produced phosphors, yet we tried to turn this drawback of the  $\text{Ca}_3\text{Y}_2\text{Si}_3\text{O}_{12}$  host material into an advantage. Namely, we expected that the reddish  $\text{Eu}^{3+}$  luminescence should be significantly broadened due to the necessary inhomogeneous broadening; consequently, this would positively influence the CRI index of the final luminescence.

Until now,  $\text{Ca}_3\text{Y}_2\text{Si}_3\text{O}_{12}$  was explored only as a host for trivalent lanthanides.<sup>16–20</sup> In this contribution, we shall present results of the fundamental research on the  $\text{Ca}_3\text{Y}_2\text{Si}_3\text{O}_{12}:\text{Eu}^{2+},\text{Eu}^{3+}$  phosphor including the VUV-UV-vis spectroscopy. Decay kinetics and temperature dependence of the phosphor luminescence characteristics will be presented

Received: July 8, 2012

Revised: November 17, 2012

Published: November 19, 2012



and discussed. Mechanisms of the various spectroscopic processes occurring in the phosphor shall be proposed.

## EXPERIMENTS AND METHODS

Calcium yttrium silicates,  $\text{Ca}_3\text{Y}_2\text{Si}_3\text{O}_{12}$ , doped with Eu were synthesized with the classic solid-state synthesis method calcining a mixture of  $\text{CaO}$  (99.9%, Aldrich),  $\text{Y}_2\text{O}_3$  (99.99%, Stanford Materials),  $\text{Eu}_2\text{O}_3$  (99.99%, Stanford Materials), and  $\text{SiO}_2$  (99.9%, Aldrich). All calculations were performed assuming that Eu replaces  $\text{Y}^{3+}$  exclusively giving formally  $\text{Ca}_3\text{Y}_{2(1-x)}\text{Eu}_{2x}(\text{SiO}_4)_3$ , where  $x = 0.001$  to 0.25. The reason for that shall be later explained.

The starting oxides were thoroughly ground with acetone as wetting medium, dried, and heated in the reducing atmosphere of 20% $\text{N}_2$ –80% $\text{H}_2$  mixture at 1400 °C for 6 h. After cooling, the materials were reground and reheated under the same conditions. The calcinations were performed in a fully programmable tube furnace, and the heating and cooling rates were 3 °C/min. The  $\text{N}_2/\text{H}_2$  mixture was prepared using gases supplied by Linde Gaz Polska. Obtained powders were white up to 1% of Eu, and they turned slightly yellowish at higher concentrations. To elaborate optimal synthesis conditions, we have tested different temperatures and times of calcinations as well as the content of hydrogen in the  $\text{H}_2/\text{N}_2$  mixture. The 1400 °C applied for 6 h was found to give materials with the lowest content of the impurity phase, whereas using the 80% $\text{H}_2$ –20% $\text{N}_2$  mixture led to a stable, most efficient overall luminescence with fully reproducible ratio of the  $\text{Eu}^{2+}$  and  $\text{Eu}^{3+}$  emissions. Consequently, we report on powders made using the optimized procedure.

Photoluminescence spectra were recorded with 0.2 to 0.5 nm resolution at room temperature (RT) and 0.05 nm at 77 K using an FSL 920 spectrometer from Edinburgh Instruments. The excitation spectra were taken with the emission monochromator slits set to 0.2 nm at RT and 0.05 nm at 77 K. A 450 W Xe-lamp was used as an excitation source. Both types of spectra were corrected for the system characteristics. Luminescence decay traces at RT and 77 K were recorded with the same instrument using its dedicated Xe flash lamp (60 W) and nitrogen nanosecond nF flash lamp as excitation sources. The RG2645 photomultiplier was exploited as a detector for emission, excitation, and decay time measurements. Decay traces obtained upon excitation with the nF flash lamp were measured with Mini Red detector (Edinburgh Instruments). The luminescence decay traces at elevated temperatures (300–600 K) were measured using the third harmonic (355 nm) of the YAG:Nd laser as an excitation source and PMT R928P side-on type photomultiplier as a detector.

The temperature-dependent luminescence spectra were measured with a homemade setup using a heating cell flowed with nitrogen (although the sample remained in the air atmosphere), a UV lamp emitting at 360 nm as an excitation source, and an Ocean Optics HR2000 CG spectrometer with resolution of ~1.2 nm. The light was collected with 74-UV collimating lens and QP800-1-SR optical fiber coupled to the spectrometer. The heating and cooling rates of 1 °C/sec were applied.

The luminescence and luminescence excitation spectra were also recorded with synchrotron radiation at the Superlum station of DESY-Hasylab in Hamburg, Germany. The emissions were recorded with a CCD camera with the resolution of ~0.05 nm and were corrected for the spectral characteristics of the detection system. The synchrotron radiation excitation spectra

were corrected for the incident light intensity using sodium salicylate as a standard. Luminescence spectra were also recorded upon excitation with 360 and 395 nm light-emitting diodes (LEDs) (supplied by OPTEL, Poland), with the power of 1.2 to 1.8 and 3 mW, respectively. The suspension of powder in ethylene glycol was deposited onto the chip of the diode. The light emitted by the phosphor was collected in transmission mode. The photoluminescence quantum efficiencies of the overall luminescence produced upon 363 and 393 nm excitation wavelengths selected from a Xe lamp with a monochromator were measured for the powder containing 15% of Eu using an Absolute PL quantum yield measurement system C9920-03G of Hamamatsu Photonics.

The X-ray diffraction (XRD) patterns were measured with a D8 Advance diffractometer (Bruker) using  $\text{Cu K}\alpha 1$  radiation ( $\lambda = 1.5406 \text{ \AA}$ ) in the range of  $2\theta = 5$ –90° with the step of  $\Delta 2\theta = 0.016^\circ$  and the counting time of 0.5 s. FTIR spectra were recorded with an IFS 66/s Bruker spectrometer in the range of 400–4000  $\text{cm}^{-1}$ . Suspensions in nujol or KBr pellets were used.

## RESULTS AND DISCUSSION

**1. Structural Measurements.**  $\text{Ca}_3\text{Y}_2\text{Si}_3\text{O}_{12}$  crystallizes in the orthorhombic crystal system with  $Pnma$  space group and is isostructural with silico-carnotite structure,  $(\text{Ca}_5(\text{PO}_4)_2\text{SiO}_4)$ . Whereas the formula is similar to that of a garnet  $(\text{A}_3\text{B}_2(\text{SiO}_4)_3)$ , the mixed occupation of A and B sites by  $\text{Ca}^{2+}$  and  $\text{Y}^{3+}$  leads to a disorder, and, as a result, the  $\text{Ca}_3\text{Y}_2\text{Si}_3\text{O}_{12}$  structure can rather be expressed as  $\text{AB}_2\text{C}_2(\text{SiO}_4)_3$ . A–C correspond to sites with nine-, eight-, and seven-fold coordination number, respectively. What is more, each site can be occupied by both  $\text{Ca}^{2+}$  and  $\text{Y}^{3+}$  ions as well. The Ca/Y ratios are ~4:1, 4:6, and 7:3 for sites A–C, respectively.<sup>16,22</sup> Structural analysis also shows that Y–O average distances are similar for the sites with seven- and eight-fold coordination (2.419 and 2.454  $\text{\AA}$ , respectively), whereas for the site with nine-fold coordination it is noticeably larger (2.616  $\text{\AA}$ ).<sup>16,22</sup> Consequently, it cannot be excluded that  $\text{Eu}^{2+}$ , due to its large ionic radius compared with  $\text{Ca}^{2+}$  and  $\text{Y}^{3+}$ <sup>21</sup> (see Table 1), may tend to preferentially occupy the nine-fold coordination symmetry site.

**Table 1. Ionic Radii of the Metal Ions Constructing the  $\text{Ca}_3\text{Y}_2\text{Si}_3\text{O}_{12}:\text{Eu}^{2+},\text{Eu}^{3+}$  Material<sup>a</sup>**

$\text{Me}^{n+}$	CN		
	7	8	9
	ionic radii ( $\text{\AA}$ )		
$\text{Ca}^{2+}$	1.06	1.12	1.18
$\text{Y}^{3+}$	0.96	1.019	1.075
$\text{Eu}^{3+}$	1.01	1.066	1.12
$\text{Eu}^{2+}$	1.20	1.25	1.30

<sup>a</sup>Data cited after ref 21.

The phase purity was checked by XRD measurements. Figure 1 compares three XRD patterns for  $\text{Ca}_3\text{Y}_2\text{Si}_3\text{O}_{12}:\text{Eu}$  containing 0.1, 3, and 25% of Eu together with the reference pattern no. 01-087-0453 from PDF-2 database. The diffractograms for other concentrations of the activator were practically identical and are not presented for better clarity of the Figure. Most of the diffraction lines are in good agreement with the expected pattern. However, the existence of an impurity phase, presumably  $\text{Ca}_4\text{Y}_8\text{O}(\text{SiO}_4)_8$  (PDF-2 no. 00-027-0093), is also

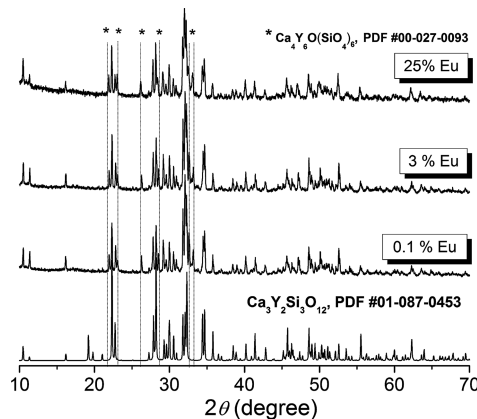


**Figure 1.** XRD patterns of  $\text{Ca}_3\text{Y}_{2(1-x)}\text{Eu}_{2x}(\text{SiO}_4)_3$  powders where  $x = 0.001, 0.03$ , and  $0.25$ , which are representative for other concentrations. Asterisks mark the lines of an impurity product, presumably  $\text{Ca}_4\text{Y}_8\text{O}(\text{SiO}_4)_8$ .

evident. From the intensities of the XRD lines related to the main and the impurity phase, we estimated the content of the latter for 6–8%. SEM and TEM images, not presented here, showed that the powders were mostly composed of rather irregular grains around 0.5 to 2  $\mu\text{m}$ , which consisted of crystallites about 100–500 nm large. Hence, the morphology was rather typical for materials treated at high temperatures.

We yet wish to mention that we also tried to prepare compositions in which the dopant would replace  $\text{Ca}^{2+}$  forming formally  $\text{Ca}_{3(1-x)}\text{Eu}_{3x}\text{Y}_2(\text{SiO}_4)_3$ . This seemed reasonable, as we wanted to stabilize divalent europium,  $\text{Eu}^{2+}$ . However, luminescence of such powders was much weaker than that from materials on which we report here,  $\text{Ca}_3\text{Y}_{2(1-x)}\text{Eu}_{2x}(\text{SiO}_4)_3$ . This was surprising at first, yet the results that we shall discuss shed more light on the possible reasons for such an effect.

**2. FTIR Spectroscopy.** FTIR spectra were measured in KBr pellets as well as in nujol in the range of  $4000$ – $400 \text{ cm}^{-1}$ , and only the latter one is presented in Figure 2, as it reveals all

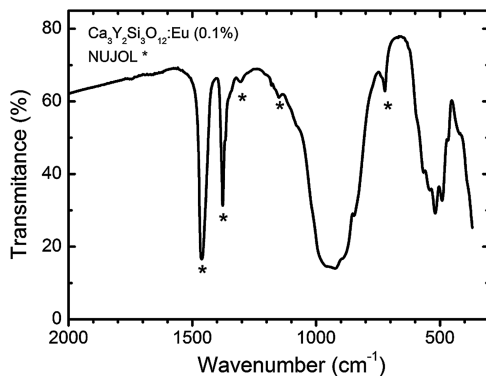


**Figure 2.** FTIR spectrum of  $\text{Ca}_3\text{Y}_{2(1-x)}\text{Eu}_{2x}(\text{SiO}_4)_3$  powders ( $x = 0.001$ ). Vibration related to nujol are marked with asterisks.

features relevant to properties of the phosphor discussed in this article. A broad absorption band with maximum around  $934 \text{ cm}^{-1}$  is attributed to symmetric and antisymmetric stretching vibrations within tetrahedral  $\text{SiO}_4$  units. At lower energies, in the range of  $650$ – $400 \text{ cm}^{-1}$ , symmetric and antisymmetric bending vibrations of  $\text{SiO}_4$  groups are easily detected. The complex shape of the structured band around  $520 \text{ cm}^{-1}$  may also indicate that modes characteristics for metal–oxygen

vibrations are located there, which is common for such types of compounds.<sup>19</sup> The absence of the absorption around  $700 \text{ cm}^{-1}$ , characteristic for the silicate network, confirms that in this material the  $\text{SiO}_4$  tetrahedrons are isolated from each other, contrary to what occurs in a similar silicate,  $\text{Ca}_3\text{Y}_2(\text{Si}_3\text{O}_9)_2$ , where  $\text{SiO}_4$  groups are linked by oxygen atoms and form ternary rings ( $\text{Si}_3\text{O}_9$ ).<sup>22</sup> Furthermore, FTIR spectra prove that synthesized materials are free of the  $\text{OH}^-$  groups or water molecules (lack of bands around  $3500$  and  $1600 \text{ cm}^{-1}$ ). It is crucial for phosphor performance because  $\text{OH}^-$  vibrations promote nonradiative relaxation pathways of excited  $\text{Eu}^{3+}$  ions.<sup>23</sup>

**3. Luminescence Spectroscopy.** **3.1. Room-Temperature UV-vis Spectroscopy.** Figure 3a presents luminescence excitation spectra of  $\text{Eu}^{3+}$  (614.4 nm) and  $\text{Eu}^{2+}$  (505 nm) emissions together with diffuse reflection spectrum of the sample containing 15% of Eu. Both excitation spectra are typical for the two ions. In the excitation spectrum of the 505 nm luminescence, quite clear dips are observed around 393 and 361 nm (less intense). They coincide with competing absorption of  $\text{Eu}^{3+}$  at these wavelengths. Importantly, these dips as well as both excitation spectra confirm that at 393 and 361 nm the excitation radiation hitting the phosphor is being shared between both luminescent species,  $\text{Eu}^{2+}$  and  $\text{Eu}^{3+}$ , and both centers then get excited. The luminescence excitation spectra expose the useful excitation wavelengths to create luminescence of  $\text{Eu}^{3+}$ ,  $\text{Eu}^{2+}$ , or both in the presented phosphor. Figure 3b shows emission spectra of the sample recorded upon stimulation into different features in the range of 270–394 nm. Practically each excitation leads to complex spectra consisting of luminescence characteristic for both  $\text{Eu}^{2+}$  and  $\text{Eu}^{3+}$  ions. The intensity ratio between them, and thus the final color of light emitted by the phosphor, obviously varies with excitation wavelength profoundly. Higher excitation energy (270 nm) favors  $\text{Eu}^{3+}$  line-type emission, which is evident because this energy coincides with the maximum of its CT excitation band. Then, moving toward lower energies,  $\text{Eu}^{2+}$  ions get stimulated increasingly more efficiently and irradiation at 340 nm produces almost exclusively the broad band emission of  $\text{Eu}^{2+}$ . Excitation around 361 nm appears suitable to get both ions excited and produce a complex luminescence composed of the broad band related to  $\text{Eu}^{2+}$  and the narrower features due to  $\text{Eu}^{3+}$  emissions. The Stokes shift of the  $\text{Eu}^{2+}$  luminescence is truly profound and reaches about  $8960 \text{ cm}^{-1}$ . Initially, we expected that  $\text{Eu}^{2+}$  would tend to substitute  $\text{Ca}^{2+}$  ions in the host lattice due to the charge and size match. It was a great surprise when it turned out that compositions made with such assumption  $((\text{Ca},\text{Eu})_3\text{Y}_2\text{Si}_3\text{O}_{12})$  were much less efficient emitters than those when Eu was assumed to replace Y ( $\text{Ca}_3(\text{Y},\text{Eu})_2\text{Si}_3\text{O}_{12}$ ). We have to remember that the host does not offer separate sites for  $\text{Ca}^{2+}$  and  $\text{Y}^{3+}$ . Instead, both ions share randomly, although with different statistics, as was mentioned in the Structural Measurements section, the three metal sites present in the lattice with CN being seven, eight, and nine. The presence of three sites may account for some enlargement of observed Stokes shift, yet its extraordinary large value ( $8960 \text{ cm}^{-1}$ ) substantiates that the system in its excited state experiences much rearrangement before radiative relaxation occurs. Such characteristics are not typical for a regular  $d \rightarrow f$   $\text{Eu}^{2+}$  luminescence and may suggest that in  $\text{Ca}_3\text{Y}_2\text{Si}_3\text{O}_{12}$  this emission possesses an anomalous nature.<sup>24,25</sup> Luminescence with similar characteristics was extensively investigated in fluoride hosts.<sup>26–29</sup> It was proposed that the anomalous

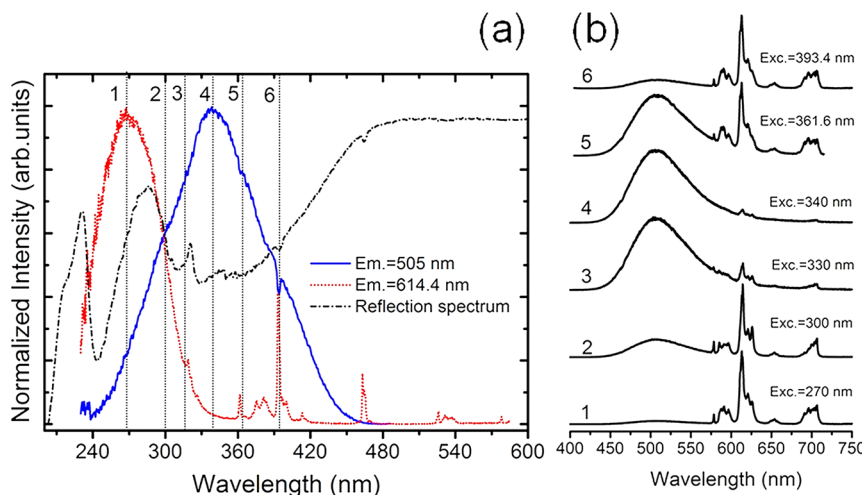


**Figure 3.** (a) Luminescence excitation spectra of Eu<sup>3+</sup> (red line) and Eu<sup>2+</sup> (blue line) emissions in Ca<sub>3</sub>Y<sub>2</sub>Si<sub>3</sub>O<sub>12</sub>:Eu (15%), together with diffuse reflection spectrum of the sample (black line). (b) Luminescence spectra measured upon excitation at different wavelengths. All spectra were taken at RT.

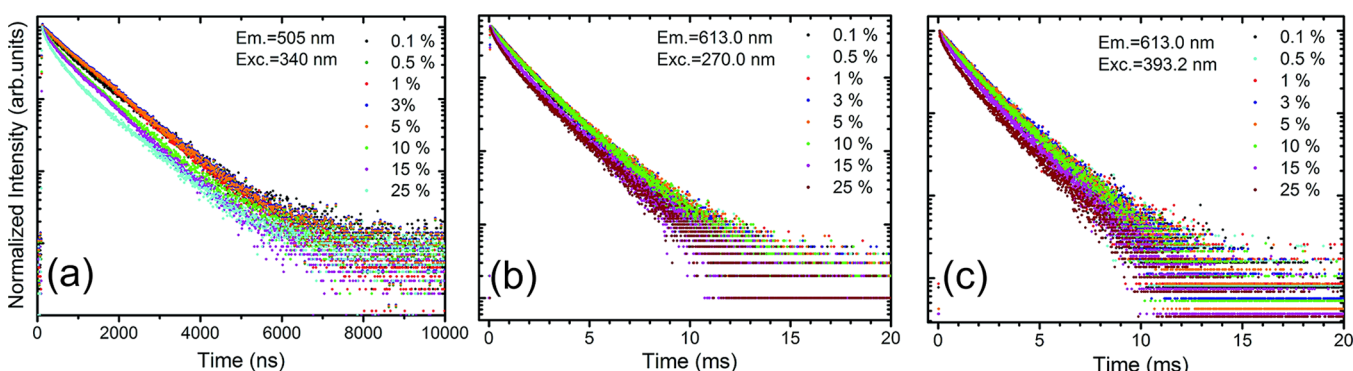


**Figure 4.** Concentration dependence of (a) luminescence decay traces of Eu<sup>2+</sup> emission recorded upon excitation at 340 nm (f → d). (b) Luminescence decay traces of Eu<sup>3+</sup> emission upon excitation at 270.0 nm (CT) and (c) upon stimulation at 393.2 nm.

emission occurs when the 5d emitting level of Eu<sup>2+</sup> locates just below the bottom of the conduction band. After excitation, autoionization takes place and the electron delocalizes over surrounding cations and finally gets trapped in a nearby defect. Then, because of a Coulomb attraction, a trapped exciton-like state is formed near the Eu<sup>2+</sup> mother ion impurity by the defect-trapped electron and the hole-like state near the Eu<sup>2+</sup> dopant. The anomalous luminescence is thus a radiative annihilation of such an excitonic entity, after which Eu<sup>2+</sup> reverts into its ground state.<sup>26,30</sup> Hence, this luminescence occurs due to the presence of Eu<sup>2+</sup> ions associated with defects. The formation of the excitonic-like entity augments the Stokes shift, and the regular d → f luminescence is precluded due to the immersion of the lowest d state within the conduction band of the host. To reveal if we really deal with such a phenomenon, we employed a temperature-dependent luminescence spectroscopy, and the results will be discussed in the next section.

Concentration dependence of the luminescent properties of the investigated phosphors within the 0.1–25% range of concentrations of the dopant was also investigated, and a clear trend was observed. With increasing the overall content of Eu, the relative intensity of Eu<sup>3+</sup> versus Eu<sup>2+</sup> luminescence got higher. This may indicate the increasing difficulty of Eu<sup>3+</sup> → Eu<sup>2+</sup> reduction with increasing content of the dopant. This is not surprising because the host must have limited capability of accommodating Eu<sup>2+</sup> replacing Y<sup>3+</sup> due to the necessity of

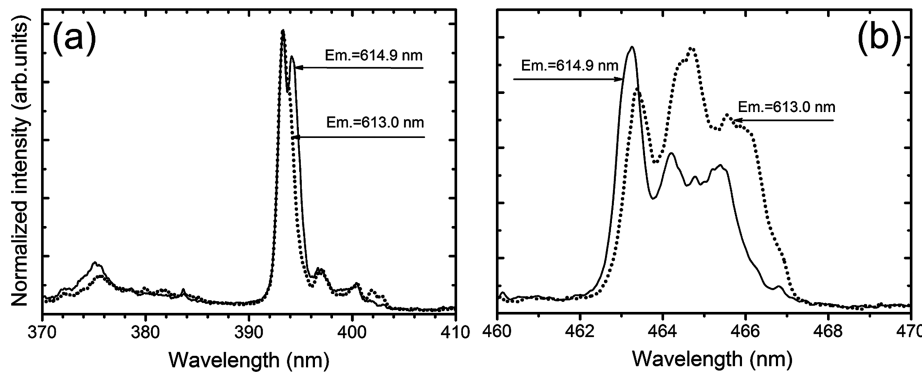
charge compensation. The presence of two types of emitting centers, Eu<sup>2+</sup> and Eu<sup>3+</sup>, may lead to energy transfer between them, especially that the <sup>5</sup>D<sub>0</sub> emitting state of the latter is positioned well below the emitting state associated with Eu<sup>2+</sup>, and the <sup>5</sup>D<sub>1</sub> level coincides with the Eu<sup>2+</sup> emission peak. The postulated Eu<sup>2+</sup> → Eu<sup>3+</sup> energy transfer might facilitate managing and controlling the luminescence color; however, the excitation spectra of Eu<sup>3+</sup> and Eu<sup>2+</sup> emissions give strong evidence that such an effect does not occur (see Figure 3a), even at the highest investigated concentration of Eu (25%). This conclusion is further confirmed by the concentration dependence of the decay kinetics of the two emissions, which we shall discuss later.

Figure 4a presents the decay traces of the Eu<sup>2+</sup> luminescence in Ca<sub>3</sub>Y<sub>2</sub>Si<sub>3</sub>O<sub>12</sub>:Eu with different Eu content (0.1–25%) upon excitation at 340 nm. In each case, the presence of two components is evident. The faster one is characterized by the decay time in the range of 0.5 to 0.7 μs, and the longer one is about 1.4 to 1.6 μs. Both values get continuously shorter with the increase in the overall Eu content, yet this effect is only minor and not evident. Definitely, not significant, concentration quenching occurs, and no proof of any energy transfer to the Eu<sup>3+</sup> ions is seen. What is also noteworthy is quite a long tail in the decay traces of Eu<sup>2+</sup> emissions, which could be connected with the existence of a defect nearby the Eu<sup>2+</sup> acting as a (temporal) trap for electrons. Their subsequent liberation

**Table 2.** Basic Kinetics Parameters Derived from Fitting of the Decay Traces of Eu<sup>3+</sup> Luminescence (613 nm) Recorded upon Different Excitation Wavelengths<sup>a</sup>

%Eu	exc. = 270 nm				exc. = 393.2 nm			
	$\tau_1$ (ms)	$\tau_2$ (ms)	magn.1%	magn.2%	$\tau_1$ (ms)	$\tau_2$ (ms)	magn.1%	magn.2%
0.1	0.96	1.70	27	73		1.70		100
0.5	0.93	1.70	23	77		1.70		100
1	0.90	1.70	22	78		1.70		100
3	0.79	1.70	17	83		1.70		100
5	0.70	1.70	12	88		1.70		100
10	0.66	1.70	12	88		1.70		100
15	0.62	1.60	19	81	0.60	1.70	16	84
25	0.46	1.60	16	84	0.52	1.70	17	83

<sup>a</sup>Standard errors of the decay times are ~10%.



**Figure 5.** Fragments of excitation spectra for Eu<sup>3+</sup> emissions located 613 and 614.9 nm recorded for Ca<sub>3</sub>Y<sub>2</sub>Si<sub>3</sub>O<sub>12</sub>:Eu (0.5%) at the temperature 77 K.

causes the appearance of the delayed emission of Eu<sup>2+</sup>. The shorter component in the Eu<sup>2+</sup> luminescence decay, which contains a roughly constant and rather small (in the range of 5–10%) fraction of the total Eu<sup>2+</sup> emission, seems to prove that a portion of Eu<sup>2+</sup> ions suffers from some quenching, which is concentration-dependent to only a minor degree and whose mechanism and source is not clear at present. Whereas at the highest concentrations contribution of this component gets slightly more profound, it is the longer constituent that is dominant over the whole range of concentrations. The decay traces of the 505 nm Eu<sup>2+</sup> emission were also recorded upon excitation at 300 and 390 nm. No significant differences were detected compared with excitation at 340 nm. Decay kinetics of the <sup>5</sup>D<sub>0</sub> Eu<sup>3+</sup> level, which gives the most prominent emission positioned around 613 nm, were investigated as the function of Eu content (0.1–25%) and excitation radiation wavelength (270 and 393.2 nm). The measured traces are presented in Figure 4b,c, and the resulting parameters obtained from the fits are given in Table 2. Up to 10% of the dopant the decays upon 393.2 nm stimulation is well-reproduced as a single exponential with the decay time of ~1.7 ms. For higher concentrations, a shorter component of ~0.6 ms appears, and it comprises 15–20% of the total emitted light. Upon excitation into the O<sup>2-</sup> → Eu<sup>3+</sup> charge-transfer transition at 270 nm the decay traces of Eu<sup>3+</sup> luminescence have two-exponential character within the whole range of concentrations. Still, the main component is ~1.7 ms, and the shorter one, ranging between 0.46 (25% of Eu) and about 0.9–1.0 ms (0.1 to 1%), comprises 12–27% of the total luminescence intensity. These characteristics suggest that Eu<sup>3+</sup> does not suffer much from quenching, although there still might be some room for improvement of its performance.

It should be noted that at RT the overall luminescence intensity increases constantly with Eu content becoming truly bright for powders activated with 5–25% of Eu. According to decay time measurements up to the Eu concentration of 10% quenching does not occur, and in the range of 15–25% it is still insignificant. Measurements of quantum efficiencies of the overall emission produced by the powder doped with 15% of Eu gave 40 and 44% upon 363 and 393 nm excitation (Xe lamp), respectively. These results are fairly encouraging because optimization of the phosphor performance was in fact not performed despite its preparation temperature. Hence, we anticipate that the phosphor may have a truly high potential.

**3.2. Low-Temperature UV-vis Spectroscopy.** We have already mentioned that there are three different symmetry sites for the metal ions in Ca<sub>3</sub>Y<sub>2</sub>Si<sub>3</sub>O<sub>12</sub> host with the CN of seven, eight, and nine and each of them is occupied by both Y<sup>3+</sup> and Ca<sup>2+</sup>, although in different ratios.<sup>16,22</sup> Consequently, we expected that the dopant ions, both Eu<sup>3+</sup> and Eu<sup>2+</sup>, would experience the different symmetry of the surroundings. Using high-resolution low-temperature spectroscopy, we tried to trace the effect. Whereas neither of the sites possesses inversion symmetry, no spectacular differences in selection rules of the transitions apply.<sup>31</sup> Hence, we had to rely on slightly different energies of the transitions in ions placed in the different symmetry sites. Low-temperature measurements (77 K) of the excitation spectra of the emission lines located around 613 and 614.9 nm (seen previously in Figure 4b) differ noticeably (Figure 5). In the range of 365–420 nm (Figure 5a), the most significant variations are connected to the excitation transition to the <sup>5</sup>D<sub>3</sub> level appearing around 393 nm. In the case of the emission monitored at 614.9 nm, two quite well-resolved lines with maxima at 393.3 and 394.2 nm were observed, whereas in

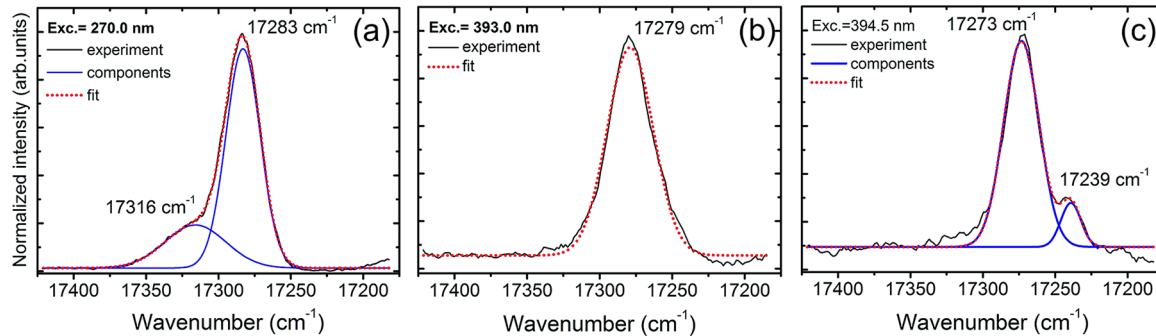


**Figure 6.** Emission spectra of  $\text{Ca}_3\text{Y}_2\text{Si}_3\text{O}_{12}:\text{Eu}$  (0.5%) in the range of  $^5\text{D}_0 \rightarrow ^7\text{F}_0$  transition recorded upon different excitation wavelengths: (a) 270, (b) 393, and (c) 394.5 nm. All spectra were measured at 77 K.

the case of emission monitored at 613 nm practically only the former component was visible. Figure 5a also exposes some other, more subtle, differences between the two excitation spectra. In the region of 460–470 nm (Figure 5b), where the hypersensitive,  $^7\text{F}_0 \rightarrow ^5\text{D}_2$ , transitions occur, the relative intensities of the numerous excitation features vary profoundly and some components are clearly present in only one of the spectra. These discrepancies reveal that  $\text{Eu}^{3+}$  ions occupying different symmetry sites are indeed present in the powders. In fact, according to the already discussed structural properties of the host, as many as three  $\text{Eu}^{3+}$  sites should be expected. Therefore, emission spectra in the  $^5\text{D}_0 \rightarrow ^7\text{F}_0$  region were taken upon semiselective (thanks to the data from Figure 5) and CT stimulation and are presented in Figure 6. Because states with  $J = 0$  get no splitting by the crystal field, just one so-called “0 → 0” emission line appears for ions occupying a specific symmetry site. Hence, more components in the  $^5\text{D}_0 \rightarrow ^7\text{F}_0$  transition region evidence the existence of  $\text{Eu}^{3+}$  ions of different surrounding symmetries. The spectra seen in Figure 6 prove that indeed emissions in the  $^5\text{D}_0 \rightarrow ^7\text{F}_0$  region change with excitation wavelengths. Finally, the spectra indicate that at least three symmetry sites of  $\text{Eu}^{3+}$  ions are present. fwhm of the main  $^5\text{D}_0 \rightarrow ^7\text{F}_0$  lines (around 17 273 and 17 283  $\text{cm}^{-1}$ ) is  $\sim 20 \text{ cm}^{-1}$ . Hence, in the region of the  $^5\text{D}_0 \rightarrow ^7\text{F}_0$  transitions upon different excitation wavelengths (270, 393.0, and 394.65 nm), we observe emission lines peaking at three different positions (577.5, 578.6–578.9, 580.1 nm), and basically all emission features seem to be inhomogeneously broadened, which prevents more detailed and unambiguous interpretation. Upon a nonselective excitation, like by means of a light-emitting diode, luminescence from all sites should appear, leading to preferred broadening of the emission structures.

**3.3. Spectroscopy under VUV Synchrotron Radiation Excitation at 10 K.** At 10 K, additional emissions came into view, as seen in Figures 7 and 8. Figure 7 presents excitation spectra monitoring the intrinsic, two broad band emissions at 340 and 405 nm, as well as the  $\text{Eu}^{3+}$  (614 nm) and  $\text{Eu}^{2+}$  (510 nm) luminescence in  $\text{Ca}_3\text{Y}_2\text{Si}_3\text{O}_{12}:\text{Eu}$  (0.5%) powder. The excitation spectrum of the 340 nm emission (black line) contains two broad overlapping bands with maxima around 170 and 200 nm. The former could be interpreted as connected to the fundamental absorption of the host. The shape of the latter is, however, puzzling. At low-energy onset, the sharp increase is characteristic of free exciton formation. However, a free-exciton absorption should be positioned just below the fundamental absorption of the host. Instead, this structure locates about 1.2 eV below the band gap energy, while typically stabilization energy of free exciton is one order of magnitude lower. Hence,

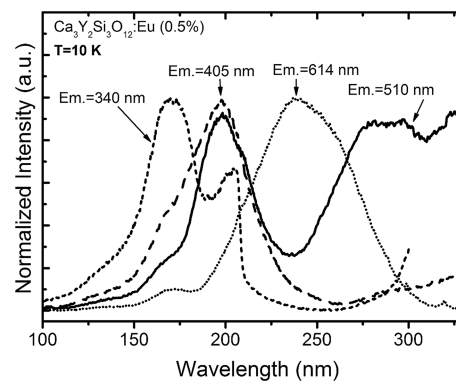


**Figure 7.** Excitation spectra for  $\text{Ca}_3\text{Y}_2\text{Si}_3\text{O}_{12}:\text{Eu}$  (0.5%) recorded at 10 K monitoring the emissions at 340 (black), 405 (red), 510 (blue), and 614 nm (green) lines.

we hypothesize that this structure might reflect the formation of an exciton localized on a defect rather. However, we should be aware, that the presence of numerous, overlapping strong absorption components in this region as well as the overlap of the broad emission bands may significantly deform the shape of excitation bands and thus may be confusing. The excitation spectrum of the luminescence at 405 nm (red line) is dominated by a strong band around 200 nm and a shoulder about 170 nm, which we have already ascribed to the fundamental absorption of the HL. Then, the excitation spectrum of  $\text{Eu}^{3+}$  luminescence located at 614 nm is composed of two bands peaking at 170 (HL) and 240 nm. Only the latter, connected to the CT of  $\text{O}^{2-} \rightarrow \text{Eu}^{3+}$ , has significant intensity. From the above data, we can estimate the band gap of  $\text{Ca}_3\text{Y}_2\text{Si}_3\text{O}_{12}$  to be  $\sim 7.3$  eV. The same value was reported for  $\text{Ca}_3\text{Sc}_2\text{Si}_3\text{O}_{12}$ .<sup>16</sup> Excitation spectrum of the  $\text{Eu}^{2+}$  luminescence positioned around 512 nm also contains a few broad features. One of them peaks around 200 nm and possesses a high-energy shoulder at 170 nm as well as a small bump at its low-energy side, which coincides with the 205–210 nm component present in the excitation spectrum of the 340 nm luminescence. This may reveal some energy transfer from the center emitting at 340 nm to the  $\text{Eu}^{2+}$  ion, which, in turn, implies that both of these centers interact, implying their spatial correlation. Another band in the excitation of  $\text{Eu}^{2+}$  emission extends from 240 nm above even 330 nm, the limit of the available excitation wavelengths at the Superlumi station. This component is assigned to the  $4f \rightarrow 5d$  transition of  $\text{Eu}^{2+}$  ions. The broad constituent located around 200 nm may reflect energy transfer from the center, presumably a defect, emitting around 405 nm to  $\text{Eu}^{2+}$ . Finally, the presence of the 200 nm band in the

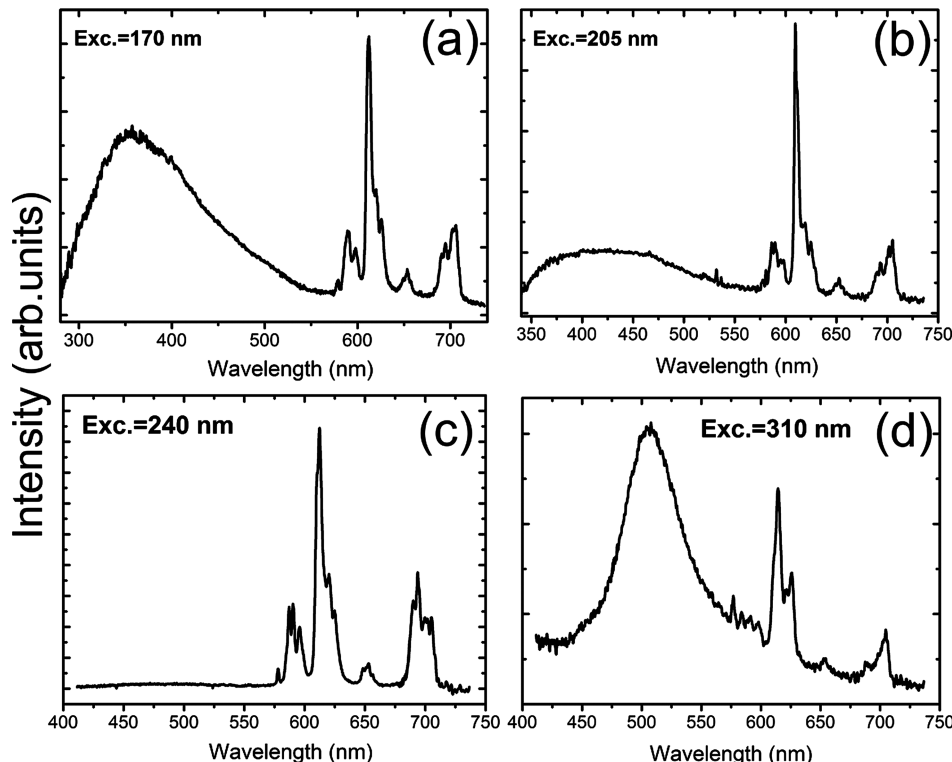


**Figure 8.** Emission spectra of  $\text{Ca}_3\text{Y}_2\text{Si}_3\text{O}_{12}:\text{Eu}$  (0.5%) recorded at 10 K upon excitation at (a) 170 (host), (b) 205 (defect), (c) 240 ( $\text{O}^{2-} \rightarrow \text{Eu}^{3+}$  CT), and (d) 310 nm ( $4f \rightarrow 5d \text{Eu}^{2+}$ ).

excitation spectrum of  $\text{Eu}^{2+}$  luminescence may result from the fact that all emissions are very broad and superimposed, and thus at 510 nm the defect luminescence (peaking around 340 nm) is also seen. Hence, excitation spectrum of the 510 nm luminescence has to necessarily contain components of all the broad emissions produced at 10 K.

Luminescence spectra recorded at 10 K upon different excitation wavelengths are presented in Figure 8. Clearly, we can distinguish as much as three broad band components and the narrower structures of  $\text{Eu}^{3+}$  luminescence at longer wavelengths. Emission spectrum upon the interband excitation (170 nm) contains a broad structured asymmetric band with a maximum at 340–350 nm and quite intense narrow features resulting from the emission of  $\text{Eu}^{3+}$  ions in the range of 580–720 nm (Figure 8a). The luminescence spectrum obtained at 300 K under the same stimulation (not presented here) is composed of a weak  $\text{Eu}^{2+}$ -related band around 505 and intense  $\text{Eu}^{3+}$  features. Excitation at 205 nm produces a similar luminescence spectrum yet with clearly reduced intensity of the host-related components located below  $\sim 450$  nm (Figure 8b). Under 240 nm irradiation, only  $\text{Eu}^{3+}$  luminescence appears (Figure 8c) because in this region hardly any other emitting centers get excited; see Figure 7. Moving the excitation toward longer wavelengths allows us to excite simultaneously the  $\text{Eu}^{2+}$  and  $\text{Eu}^{3+}$  centers (Figure 8d). Summarizing these findings, we conclude that energy of electrons excited all the way up to the conduction band (170 nm) is shared between a number of luminescent entities among which the  $\text{Eu}^{2+}$  seems to be the least effective in its interception. At low temperature, below about 450–500 nm, two emissions appear, and the one at 340 nm is much stronger. A similar feature (340 nm) was observed in  $\text{Ca}_3\text{Sc}_2\text{Si}_3\text{O}_{12}$ .<sup>16,32</sup> However, when the temperature is raised up to  $\sim 300$  K and the mobility of carriers gets higher only the

$\text{Eu}^{2+}$  and  $\text{Eu}^{3+}$  are fed by the energy deposited in the host (these spectra are not presented), yet such excitation is still rather inefficient, and neither of the two ions produces powerful luminescence upon stimulation of the host material. The low-temperature experiments with the use of synchrotron radiation proved the presence of defect(s) able to produce luminescence at short wavelengths, in the UV and violet parts of the spectrum. These defects may well participate in the generation of the abnormal luminescence of  $\text{Eu}^{2+}$ , as previously mentioned. VUV spectroscopy gives us a consistent picture of the relation between the energy levels of intentionally introduced impurities and other entities involved in the luminescence processes. This knowledge will be very helpful in understanding a peculiar temperature dependence of  $\text{Eu}^{2+}$  and  $\text{Eu}^{3+}$  luminescence in the  $\text{Ca}_3\text{Y}_2\text{Si}_3\text{O}_{12}$  host.

**3.4. Luminescence at Elevated Temperatures (298–573 nm).** One of the most important parameter in the case of phosphors pretending to have application in the pc-WLEDs is the stability of their luminescence at higher temperatures because high-power WLEDs may warm up to about 150–200 °C. Therefore, we measured the temperature dependence of the  $\text{Eu}^{3+}$  and  $\text{Eu}^{2+}$  emissions decay times as well as the luminescence spectra and their intensities up to 300 °C. Such measurements were done for samples with low (0.5%) Eu content to determine the intrinsic quenching temperature as well as for the powder containing high Eu concentration (10%) to trace possible thermally induced spectroscopic processes when the separation of the optically active ions is much lower. A similar approach was reported in the case of YAG:Ce showing that its intrinsic quenching appears at impressively high temperatures (even above 700 K).<sup>33</sup> However, in materials with higher Ce<sup>3+</sup> concentrations (1–5%, as commercially used), the emission intensity decreased steadily already above 400 K,<sup>34</sup>

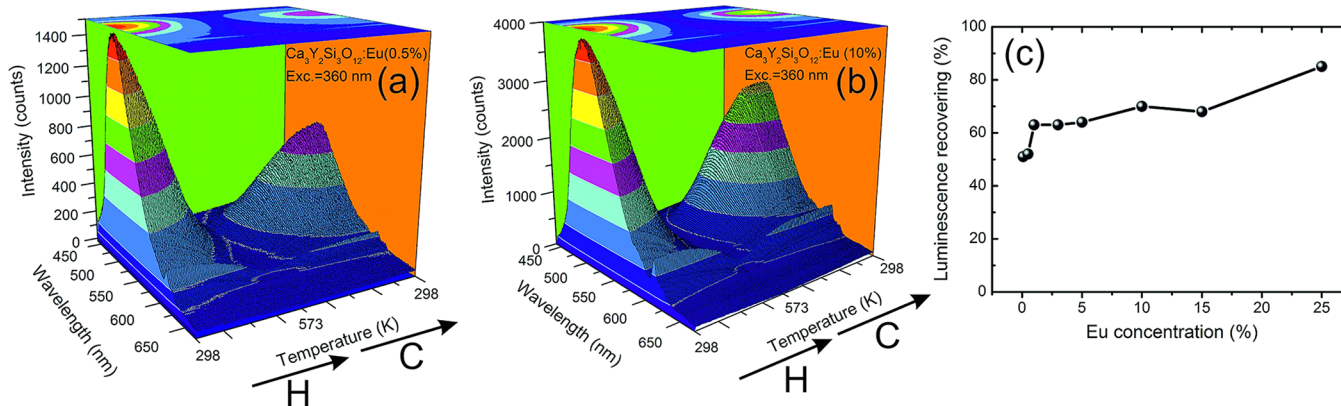


**Figure 9.** Three-dimensional graphs of the emission spectra of  $\text{Ca}_3\text{Y}_2\text{Si}_3\text{O}_{12}\text{-Eu}$  0.5% (a) and 10% (b) measured in the range of 298–573 (H; heating) and 573–298 K (C; cooling). (c) Concentration dependence of the percentage of luminescence recovery during the whole cycle of heating–cooling procedure. (See the text for details.)

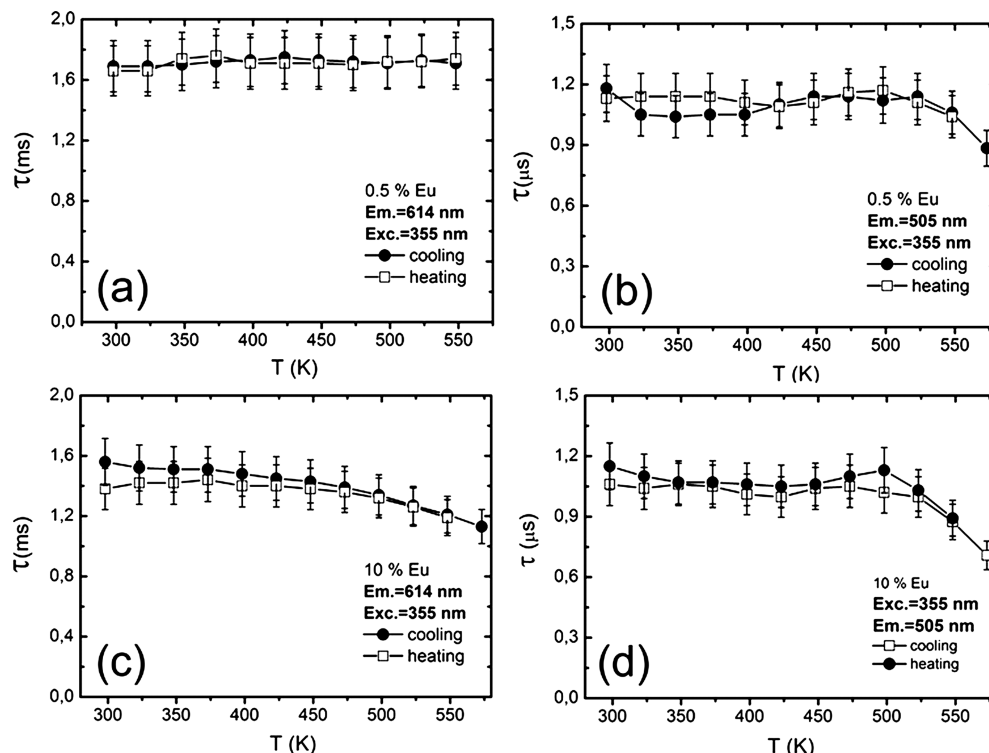


**Figure 10.** Dependence of decay times of  $\text{Eu}^{2+}$  and  $\text{Eu}^{3+}$  emissions during the heating (298–573 K) and cooling (573–298 K) for samples with 0.5% Eu (a,c) and 10% Eu (b,d). The bars give the estimated errors of the calculated values.

which was revealed to result from a thermally activated concentration quenching.<sup>33</sup> In Figure 9, we present variations in luminescence spectra excited at 360 nm upon heating from RT to 573 K and subsequent cooling back to RT of the powder containing 0.5% of Eu. It is immediately seen that upon heating the broad-band  $\text{Eu}^{2+}$  emission intensity decreases quickly and practically disappears (while measured with our low sensitivity CCD spectrometer) already about 500 K. During the subsequent cooling, this luminescence comes into view again and successively becomes stronger, yet at RT it regains only ~50% of its original intensity. Repeated measurements (on fresh portions of samples) confirmed this effect. It is easy to note that at higher temperatures the peak intensity of this luminescence moves slightly toward shorter wavelengths, as expected for the  $5d \rightarrow 4f$  luminescence. Upon such excitation

(360 nm), emission of  $\text{Eu}^{3+}$  is rather weak from the very beginning. Yet, its intensity weakens only slightly during the heating. Analogous measurements were performed for all other concentrations of the activator and, qualitatively, comparable results were obtained. Figure 9b gives the changes in powder doped with 10% of Eu. At higher concentrations, the intensity ratio of  $\text{Eu}^{3+}/\text{Eu}^{2+}$  emissions at RT was clearly stronger, which seems to reflect the increasing relative content of  $\text{Eu}^{3+}$  versus  $\text{Eu}^{2+}$  ions, as we have already mentioned. At higher Eu concentrations, the loss of  $\text{Eu}^{2+}$  luminescence after the whole cycle (RT  $\rightarrow$  573 K  $\rightarrow$  RT) was significantly lower. At 25% of Eu, it reached 15%, as is seen in Figure 9c. Another heating–cooling cycle, independently of the Eu content, did not lead to further decrease in the  $\text{Eu}^{2+}$  emission at RT. Hence, all loss happened during the first heat-treatment. Even prolonged

heating at 575 K (a few hours) combined with exposure to UV photons did not additionally alter the Eu<sup>2+</sup> RT luminescence intensity.

Figure 10 presents complementary information, namely, the decay times of Eu<sup>3+</sup> and Eu<sup>2+</sup> luminescence during the heating (298–573 K) and subsequent cooling (573–298 K). Figure 10a proves that in the diluted composition (0.5%) the RT decay time of the red Eu<sup>3+</sup> luminescence is ~1.6 ms. (This value is 0.1 ms shorter than that reported in Section 3.1, which was measured using a different setup; see the section: Experiments and Methods.) It remains unaffected upon heating up to 575 K as well as during the subsequent cooling to RT. This result is in reasonably good accord with the behavior of Eu<sup>3+</sup> ion luminescence intensity presented in Figure 9a, where this emission intensity was only slightly reduced at higher temperatures. For the heavily doped powder (10%, Figure 10c), the RT decay time was found to be about 1.5 to 1.6 ms, which is very similar to the diluted composition, yet, with increasing temperature, some shortening of the decay time appears and continues up to 575 K, the highest temperature investigated, when it gets reduced to ~1.2 ms. This effect may be connected to the growing probability of energy migration with increasing temperature and thus with rising prospect to dissipate the energy to a luminescence killing center (a defect) located nearby Eu<sup>3+</sup>. During the cooling procedure, the decay time regains values very similar to those found upon heating. Hence, also in this case, the Eu<sup>3+</sup> luminescence decay time behavior is in accord with the temperature dependence of the intensity of the Eu<sup>3+</sup> emission presented in Figure 9b. For the broad-band Eu<sup>2+</sup> luminescence the situation is more complex. The decay time for the diluted composition (0.5%) is about 1.0 to 1.1  $\mu$ s at RT. This value is pretty stable up to ~525 K, when the trace still reasonably follows the single exponential form. At yet higher temperatures a quenching becomes evident and increasing contribution from a short component appears. Finally, even the longer constituent shortens, proving that basically all emitting ions suffer, although to a different extent, from quenching of their luminescence at the highest investigated temperature (575 K). Upon cooling, the decay traces at specific temperatures meet those obtained during heating, and, from 500 K to RT, the single exponential behavior is observed with the time constants around 1.0 to 1.1  $\mu$ s. Clearly, the variations of the Eu<sup>2+</sup> luminescence decay time with temperature are much different from changes in the emission intensity presented already in Figure 9a. Similar behavior is observed for the high-concentration system (10%). Up to 500 K, the decay time is also 1.0 to 1.1  $\mu$ s, and only at 500 K do the first indications of quenching become evident. A further growth of temperature makes the quenching more effective and not only does the short component become yet shorter but the longer one gets reduced too. Hence, as could be expected, the higher content of the activator led to noticeably more profound quenching of the Eu<sup>2+</sup>-related emission. At least up to ~400 K, the decay time of this luminescence in both compositions was similar and constant, indicating no obvious quenching in such conditions. The initial impression is that the data presented in Figures 9 and 10 are *not* consistent in terms of the Eu<sup>2+</sup> luminescence. Its intensity decreases quickly with temperature, whereas its decay time is quite constant up to about 400–500 K. Upon cooling, the decay time mirrors the values obtained upon heating, whereas the intensity recovers only partially (50–85%, depending on the Eu concentration, Figure 9c). It seems that an increasing fraction of the Eu<sup>2+</sup> ions is being

“switched off” upon heating and only part of them is able to regain the capability to luminesce after subsequent cooling. It is tempting to blame an oxidation of Eu<sup>2+</sup> to Eu<sup>3+</sup> for the reduced Eu<sup>2+</sup> emission efficiency at higher temperatures. However, if that would be a main mechanism standing behind this phenomenon upon subsequent cooling, then the material would not regain the ability to emit by means of Eu<sup>2+</sup> because this luminescent center would not exist anymore. However, the broad Eu<sup>2+</sup> emission indeed reappears, although its intensity after cooling back to RT is lower than that before heating. Hence, although we do not exclude that some of Eu<sup>2+</sup> ions may indeed get oxidized, this is not the process standing behind the data presented in Figure 9. Then, what could be an alternative mechanism staying in agreement with the observed phenomena depicted in Figures 9 and 10? Let us recall the extraordinary Stokes shift of Eu<sup>2+</sup> luminescence, which indicates that it is connected with a particularly large change in the average equilibrium distance(s) between the emitting metal ion and its ligands in the ground and excited states. Such a situation may easily occur when Eu<sup>2+</sup> resides in a site originally occupied by a much larger ion (for example Ba<sup>2+</sup>). However, this is not our case, as both Ca<sup>2+</sup> and Y<sup>3+</sup> are smaller than Eu<sup>2+</sup>, making the latter tightly surrounded in the host by its ligands, which restricts their capability of significant movement and repositioning. Another situation leading to the enlargement of the Stokes shift is the involvement of a Eu<sup>2+</sup>-neighboring entity in the participation in the excited state, which spreads this state over a space well exceeding a single atom/ion of the activator. This is a typical situation in charge-transfer transitions, in which the excitation state is extended over both the ligand and the metal, yet an activator with a nearby located defect may experience a similar possibility. Namely, electron excited to the 5d state may get coupled to the defect state either by means of tunneling or getting there through the conduction band if the 5d state is located within or close to it. Consequently, the excited electron appears mostly at the adjacent defect, leaving a hole-like state near/at the Eu<sup>2+</sup> ion. The existence of a defect having such a functionality was apparently proved by synchrotron radiation experiments (Figures 7 and 8). Moreover, the broad band Eu<sup>2+</sup> emission was efficient only when the Eu<sup>2+</sup> was forced to replace Y<sup>3+</sup>, which immediately created the need for compensation of the lower charge, hence forming a defect. In the reducing conditions applied in the fabrication process it might be easily achieved by O<sup>2-</sup> vacancy, which in turn, having a positive net charge, could be an effective electron-trap defect and should tend to locate in the vicinity of Eu<sup>2+</sup>. Clearly, we have good reasons to anticipate that [Eu<sup>2+</sup>-O<sup>2-</sup><sub>vac</sub>] clusters (pairs of point defects) are present in the Ca<sub>3</sub>Y<sub>2</sub>Si<sub>3</sub>O<sub>12</sub>:Eu powders fabricated in reducing atmosphere. Therefore, electron excited to the 5d level of Eu<sup>2+</sup> may escape its mother ion and get trapped in the O<sup>2-</sup><sub>vac</sub> defect. Thus, after excitation, a [(O<sup>2-</sup><sub>vac</sub>-e)-(Eu<sup>2+</sup>-h)]\* entity with excessive energy would be formed. Its formation would be facilitated by the Coulomb attraction of the charges: an electron, e, bound to O<sup>2-</sup><sub>vac</sub> and a hole, h, localized at Eu<sup>2+</sup>. Annihilation of the [(O<sup>2-</sup><sub>vac</sub>-e)-(Eu<sup>2+</sup>-h)]\* exciton-like excited state would make the broad-band luminescence with a large Stokes shift, as observed. Because this might occur at each of the three metal sites, an enhanced broadening of the overall luminescence band related to Eu<sup>2+</sup> would take place, exactly as it is observed. Upon heating, when the decay time is practically constant but the luminescence intensity drops down quickly, the formation of the [(O<sup>2-</sup><sub>vac</sub>-e)-(Eu<sup>2+</sup>-h)]\* excitonic state seems to be

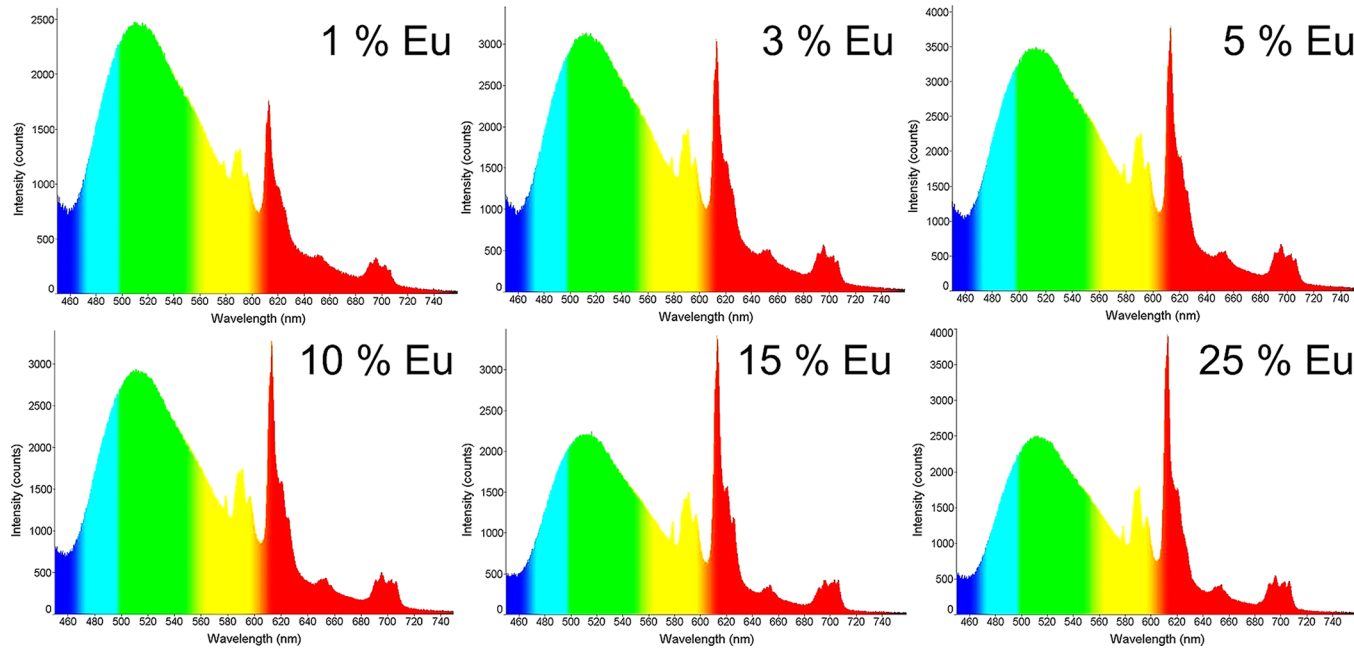


**Figure 11.** RT emission spectra of  $\text{Ca}_3\text{Y}_2\text{Si}_3\text{O}_{12}:\text{Eu}$  with different Eu contents obtained upon excitation with 395 nm LED.

continuously less probable, reducing the efficiency of the broad band luminescence. What is more, the increasing temperature could easily cause diffusion of oxygen into the O vacancies coupled to  $\text{Eu}^{2+}$ . This would reduce the number of  $[\text{O}_{\text{vac}}\text{-}\text{Eu}^{2+}]$  clusters necessary to produce the broad band abnormal luminescence of  $\text{Eu}^{2+}$ , as described above. This does not indisputably mean that  $\text{Eu}^{2+}$  gets oxidized to  $\text{Eu}^{3+}$ , but as a consequence of filling *some* of the  $\text{O}^{2-}_{\text{vac}}$  after cooling, the efficiency of this luminescence would not meet its value characteristic for the freshly prepared powder. We do not exclude that sintered ceramics, where the O diffusion is necessarily less efficient at the moderate temperatures than in fine powders, would be less susceptible for the  $\text{Eu}^{2+}$  emission intensity drop upon heating. This, however, awaits experiments to be elucidated.

**3.5. Luminescence upon 395 nm Diode Excitation.** In Section 3.1, we showed that the ratio of  $\text{Eu}^{2+}/\text{Eu}^{3+}$  emission intensities can be tuned by varying the stimulation energy. In Figure 11, we present a series of emission spectra of the  $\text{Ca}_3\text{Y}_2\text{Si}_3\text{O}_{12}:\text{Eu}$  phosphor powders with different content of the dopant upon 395 nm LED excitation. Independently, on the Eu content, the spectra consist of two types of previously described emissions ( $\text{Eu}^{2+}$ ,  $\text{Eu}^{3+}$ ). It appeared that coupling the phosphor to a near-UV LED (395 nm) allows getting luminescence whose color is concentration-dependent. The emission color changes continuously from greenish white to yellowish white as the concentration of the dopant increases. (See also Table 3.) Clearly, compared with the regular white light, emission from  $\text{Ca}_3\text{Y}_2\text{Si}_3\text{O}_{12}:\text{Eu}$  upon 395 nm LED excitation lacks some blue-violet and some red components.

Excitation with 360-diode creates emission with strong deficiency of the red  $\text{Eu}^{3+}$  luminescence, even for the highest concentrations of Eu (25%). This occurs because there is practically no  $\text{Eu}^{2+} \rightarrow \text{Eu}^{3+}$  energy transfer (besides an inefficient radiative transfer through reabsorption of the  $\text{Eu}^{2+}$  emission by  $\text{Eu}^{3+}$  ions). Hence, to get good balance between the  $\text{Eu}^{2+}$  and  $\text{Eu}^{3+}$  emissions, excitation with a ~395 nm LED is needed.

**Table 3. Chromaticity Coordinates ( $x$ ,  $y$ ) Calculated Regarding Blackbody Illuminant for  $\text{Ca}_3\text{Y}_2\text{Si}_3\text{O}_{12}:\text{Eu}$  (1–25%) upon 395-LED Excitation**

% Eu	$x$	$y$
1	0.3186	0.5091
3	0.3338	0.5028
5	0.3339	0.5057
10	0.3345	0.5064
15	0.3487	0.5029
25	0.3559	0.5009
white light	0.333	0.333

## CONCLUSIONS

$\text{Ca}_3\text{Y}_2\text{Si}_3\text{O}_{12}:\text{Eu}$  was synthesized with a ceramic method in the reducing atmosphere of  $\text{N}_2\text{-H}_2$  mixture. UV-vis luminescence spectroscopy indicated that europium exists in the HL at two valence states, as  $\text{Eu}^{3+}$  and  $\text{Eu}^{2+}$ . The spectroscopic characteristic of  $\text{Eu}^{2+}$  luminescence suggest that it has a rather anomalous character with a neighboring defect, presumably an O vacancy, participating in the emission. It was shown that depending on the wavelength of stimulating radiation the  $\text{Eu}^{3+}$  and  $\text{Eu}^{2+}$  ions can be excited either separately or simultaneously. The latter can also be done with 395 nm LED. VUV-UV synchrotron measurements revealed that at 10 K not only does Eu-associated emission occurs but also intrinsic and defect-related ones contribute to the overall luminescence of  $\text{Ca}_3\text{Y}_2\text{Si}_3\text{O}_{12}:\text{Eu}$ . It was also shown that the excited host is able to transfer its energy mainly to  $\text{Eu}^{3+}$ , and even then, according to excitation spectra, this is not an efficient process. A continuous decrease in the  $\text{Eu}^{2+}$  luminescence intensity in  $\text{Ca}_3\text{Y}_2\text{Si}_3\text{O}_{12}:\text{Eu}^{2+},\text{Eu}^{3+}$  powders above RT was inferred to have its source in a reduced probability of formation of the  $[(\text{O}^{2-}_{\text{vac}}\text{-e})\text{-}(\text{Eu}^{2+}\text{-h})]^*$  excitonic state generated with the use of the  $[\text{Eu}^{2+}\text{-O}_{\text{vac}}]$  clustered point defects. An incomplete recovery of the original luminescence intensity of  $\text{Eu}^{2+}$  after the RT–573 K–RT heating–cooling cycle was assigned to a partial filling of the O-vacancies at elevated temperatures. The thermal

quenching of Eu<sup>2+</sup> luminescence, as defined by shortening of its decay time, was found to start above 500 K. The luminescence upon excitation with 395-diode revealed that the final color of the light emitted by our phosphors was close to white but with noticeable hue of green or yellow color depending on the overall Eu content. Hence, it lacked some violet-blue and red components to become naturally white. A relatively high quantum efficiency of 40–44% and justified anticipation of possible improvement make Ca<sub>3</sub>Y<sub>2</sub>Si<sub>3</sub>O<sub>12</sub>:Eu<sup>2+</sup>,Eu<sup>3+</sup> composition an interesting phosphor.

## AUTHOR INFORMATION

### Corresponding Author

\*E-mail: eugeniusz.zych@chem.uni.wroc.pl. Tel: +48 71 3757248. Fax: +48 71 3282348.

### Notes

The authors declare no competing financial interest.

## ACKNOWLEDGMENTS

We thank Dr. Adam Watras for quantum efficiency measurements and Dr. Lukasz Marciniaik for the temperature-dependent luminescence decay kinetics measurements. We wish to thank Professor Przemyslaw Dereń for helpful discussions. This work was supported by POIG.01.01.02-02-006/09 project cofunded by European Regional Development Fund within the Innovative Economy Program. Priority I, Activity 1.1. Subactivity 1.1.2, which is gratefully acknowledged. Partial support through DESY HasyLab Grant no. II-20090289 EC and Minister of Science and Higher Education Grant no. N N209 044839 are also acknowledged.

## REFERENCES

- (1) Xia, Z.; Zhuang, J.; Liu, H.; Liao, L. *J. Phys. D: Appl. Phys.* **2012**, *45*, 015302-1–015302-7.
- (2) Smet, P. F.; Parmentier, A. B.; Poelman, D. *J. Electrochem. Soc.* **2011**, *158* (6), R37–R54.
- (3) Mueller-Mach, R.; Mueller, G.; Krames, M. R.; Höppe, H. A.; Stadler, F.; Schnick, W.; Justel, T.; Schmidt, P. *Phys. Stat. Sol. (a)* **2005**, *202* (9), 1727–1732.
- (4) Bachmann, V.; Meijerink, A.; Ronda, C. *J. Lumin.* **2009**, *129*, 1341–1346.
- (5) Dai, Q.; Foley, M. E.; Bresliske, C. J.; Lita, A.; Strouse, G. F. *J. Am. Chem. Soc.* **2011**, *133*, 15475–15486.
- (6) Ellens, A.; Jermann, F.; Kummer, F.; Ostertag, M.; Zwachska, F. U.S. Pat. No. 6,504,179 B1, 2003.
- (7) Bogner, G.; Botty, G.; Braune, B.; Hintzen, H. T.; van Krevel, J. W. H.; Waitl, G. U.S. Pat. No. 6,649,946 B2, 2003.
- (8) Srivastava, A. M.; Comanzo, H. A. U. S. Pat. No. 7,015,510 B2, 2006.
- (9) Radkov, E.; Setlur, A. A. U.S. 2007/0276606 A1, 2007.
- (10) Sohn, J. R.; Yoon, C. S.; Kwak, C. H.; Park, I. W. U.S. 7,804,239 B2, 2010.
- (11) Lin, C. C.; Liu, R. S. *J. Phys. Chem. Lett.* **2011**, *2*, 1268–1277.
- (12) Armelao, L.; Bottaro, G.; Quici, S.; Scalera, C.; Cavazzini, M.; Accorsi, G.; Bolognesi, M. *ChemPhysChem* **2010**, *11*, 2499–2502.
- (13) Justel, T. Luminescent Materials for Phosphor-Converted LED. In *Luminescence: From Theory to Applications*; Ronda, C., Ed.; Wiley-VCH: Weinheim, Germany, 2008.
- (14) Ye, S.; Xiao, F.; Pan, Y. X.; Ma, Y. Y.; Zhang, Q. *Mater. Sci. Eng., R* **2010**, *71*, 1–34.
- (15) Srivastava, A. M.; Comanzo, H. A. U. S. Pat. No. 7,015,510 B2, 2006.
- (16) Ivanovskikh, K. V.; Meijerink, A.; Piccinelli, F.; Speghini, A.; Zinin, E. I.; Ronda, C.; Bettinelli, M. *J. Lumin.* **2010**, *130*, 893–901.
- (17) Piccinelli, F.; Speghini, A.; Mariotto, G.; Bovo, L.; Bettinelli, M. *J. Rare Earth.* **2009**, *27*, 555–559.
- (18) Bandi, V. R.; Nien, Y. T.; Chen, I. G. *J. Appl. Phys.* **2010**, *108*, 023111-1–023111-4.
- (19) Bandi, V. R.; Nien, Y. T.; Lu, T. H.; Chen, I. G. *J. Am. Ceram. Soc.* **2009**, *92*, 2953–2956.
- (20) Bandi, V. R.; Grandhe, B. K.; Jang, K.; Lee, H. S.; Yi, S. S.; Jeong, J. H. *Ceram. Int.* **2011**, *37*, 2001–2005.
- (21) Shannon, R. D. *Acta Crystallogr., Sect. A* **1976**, *32*, 751–767.
- (22) Yamane, H.; Nagasawa, T.; Shimada, M.; Endo, T. *Acta Crystallogr., Sect. C* **1997**, *53*, 1367–1369.
- (23) Zych, E. *Opt. Mater.* **2001**, *16*, 445–452.
- (24) Dorenbos, P. *J. Lumin.* **2003**, *104*, 239–260.
- (25) Shionoya, S.; Yen, W. M. *Phosphors Handbook*; CRC Press: Boca Raton, FL, 1990.
- (26) McClure, D. S.; Pedrini, C. *Phys. Rev. B* **1985**, *32*, 8465–8468.
- (27) Cramer, L. P.; Cumby, T. D.; Leraas, J. A.; Langford, S. C.; Dickinson, J. T. *J. Appl. Phys.* **2005**, *97*, 103533-1–103533-6.
- (28) Gatch, D. B.; Boye, D. M.; Shen, Y. R.; Grinberg, M.; Yen, Y. M.; Meltzer, R. S. *Phys. Rev. B* **2006**, *74*, 195117-1–195117-6.
- (29) Su, F. H.; Chen, W.; Ding, K.; Li, G. H. *J. Phys. Chem. A* **2008**, *112*, 4772–4777.
- (30) Dorenbos, P. *J. Phys.: Condens. Matter* **2003**, *15*, 265–2665.
- (31) Wybourne, B. G. *Spectroscopic Properties of Rare Earths*; Interscience: New York, 1965.
- (32) Piccinelli, F.; Speghini, A.; Ivanovskikh, K.; Meijerink, A.; Ronda, C.; Bettinelli, M. *Mater. Res. Soc. Symp. Proc.* **2009**, *1111*, D08–D07.
- (33) Bachmann, V.; Ronda, C.; Meijerink, A. *Chem. Mater.* **2009**, *21*, 2077–2084.
- (34) Setlur, A. A.; Heward, W. J.; Gao, Y.; Srivastava, A. M.; Chandran, R. G.; Shankar, A. V. *Chem. Mater.* **2006**, *18*, 3314–3322.